REPORT DOCUMENTATION PAGE

Form Approved
OMB NO. 0704-0188

1. AGENCY USE ONLY (Leave Blank)	2. REPORT DATE	3. REPORT TYPE AND DATES COVERED
	April 26, 2003	Final, 8/1/2002-1/31/2003

4. TITLE AND SUBTITLE
Experimental Investigation of Upstream Boundary Layer Acceleration on Unsteadiness of Shock-Induced Separation

5. FUNDING NUMBERS
DAAD 19-02-1-0294

6. AUTHOR(S)
David S. Dolling and Noel T. Clemens

7. PERFORMING ORGANIZATION NAME(S) AND ADDRESS(ES)
The University of Texas at Austin

8. PERFORMING ORGANIZATION REPORT NUMBER

9. SPONSORING / MONITORING AGENCY NAME(S) AND ADDRESS(ES)
U. S. Army Research Office
P.O. Box 12211
Research Triangle Park, NC 27709-2211

10. SPONSORING / MONITORING AGENCY REPORT NUMBER
Proposal number
44073-EG-II

11. SUPPLEMENTARY NOTES
The views, opinions and/or findings contained in this report are those of the author(s) and should not be construed as an official Department of the Army position, policy or decision, unless so designated by other documentation.

12 a. DISTRIBUTION / AVAILABILITY STATEMENT
Approved for public release; distribution unlimited.

12 b. DISTRIBUTION CODE

13. ABSTRACT (Maximum 200 words)

This project was aimed at understanding the fundamental cause of the low frequency unsteadiness present in shock-induced turbulent separated flows. A new multi-camera, multi-laser PIV system was used to capture wide-field images of the velocity field in a Mach 2 compression ramp interaction. The PIV was acquired simultaneously with fast-response pressure measurements to identify the shock-foot location at the same time that the PIV data were captured. The measurements showed that the global structure of the interaction was substantially different depending on the location of the separation shock foot. For example, when the shock is upstream, the scale of the separated flow, the velocity fluctuations and the domain of perturbed flow, are all substantially larger than when the shock-foot is located downstream. Most importantly, a clear correlation was observed between the thickness and velocity profile in the upstream boundary layer and the shock foot position. A new technique for measuring the upstream boundary layer acceleration by using two-frame time-sequenced PIV was also developed. This involved developing new hardware and software tools, and conducting preliminary calibration experiments. This work has shown the feasibility of correlating the upstream acceleration to the shock motion and these measurements will be made in future work.

14. SUBJECT TERMS	15. NUMBER OF PAGES
Fluid dynamics, turbulence, supersonic flow	22
	16. PRICE CODE

17. SECURITY CLASSIFICATION OR REPORT	18. SECURITY CLASSIFICATION ON THIS PAGE	19. SECURITY CLASSIFICATION OF ABSTRACT	20. LIMITATION OF ABSTRACT
UNCLASSIFIED	**UNCLASSIFIED**	**UNCLASSIFIED**	**UL**

REPORT DOCUMENTATION PAGE (SF298)
(Continuation Sheet)

Table of Contents

Problem Statement

A flow of particular interest to the U.S. Army is shock-wave induced turbulent boundary layer separation, which occurs around missile fins, base flows and rotor blades. A common feature of these flows is that they are highly unsteady and are characterized by large-scale pulsation at frequencies that are an order of magnitude, or more, below the characteristic frequency of the turbulence. Due to the complex nature of these flows and the high Reynolds numbers at which they exist, they remain largely beyond the capabilities of current theoretical and computational techniques. Therefore, at this stage, it is unlikely that they key phenomena and mechanisms responsible for the flow field unsteadiness will emerge solely from computation. This highlights the crucial role that advanced measurements must play if a fundamental understanding of the physics of such complex flow fields is to be attained.

This project was aimed at understanding the fundamental cause of the low frequency unsteadiness present in shock-induced turbulent separated flows. In particular, it was based on the important result found in a previous study of Mach 5 interactions that velocity fluctuations in the upstream boundary layer were strongly correlated with shock foot motion. The goal of this work was to determine whether this same mechanism is important in Mach 2 compression ramp interactions and to investigate the hypothesis that flow acceleration in the upstream boundary layer is strongly correlated with shock-foot motion.

The Mach 2 compression ramp interactions were studied using a multi-camera, multi-laser PIV system that was recently developed under ARO sponsorship. To simultaneously monitor the shock foot location, the PIV was acquired simultaneously with fast response pressure measurements under the intermittent region. The wide-field PIV enabled the imaging of the entire shock wave / boundary layer interaction, spanning the upstream boundary layer, intermittent region, separated flow and the boundary layer that reattaches on the ramp face. Ensemble average PIV images, conditioned upon the shock-foot location within the intermittent region revealed several very important findings. First of all, the global structure of the interaction was found to be substantially different depending on the location of the separation shock foot. When the shock is upstream, the scale of the separated flow, the velocity fluctuations and the domain of perturbed flow, are all substantially larger than when the shock-foot is located downstream. Perhaps the most important finding was that the upstream boundary thickness was seen to be correlated with the shock-foot position. Specifically, the upstream boundary layer is thicker when the shock foot is upstream and thinner when the shock foot is downstream. This result suggests that unsteadiness of the interaction is strongly coupled to variations in the upstream boundary layer. This result is different than what was found previously in Mach 5 interactions, but the reason for this difference is not know at this time.

It is believed that flow acceleration, or the rate of change of the velocity profile, in the upstream boundary layer, may provide an even stronger correlation with shock-foot motion. Over the course of this grant the capability to investigate this hypothesis was developed. This entailed the development of two-image time-sequenced PIV, where the time between images could be varied between 30 and 100 μs. This is a difficult technique because it requires careful timing of two lasers and two cameras, the application of a new electronic shuttering device, and the ability to register the two cameras to sub-pixel accuracy. The necessary development work has been accomplished and experiments are currently underway to test the acceleration hypothesis.

Participating Personnel

David S. Dolling - Professor

Noel T. Clemens - Associate Professor

Yongxi Hou – Graduate Research Assistant, Ph.D expected Dec. 2003

Publications and Technical Reports

1. Hou, Y.X., Clemens, N.T. and Dolling, D.S., "Development of a Multi-Camera PIV Imaging System for Studies of Shock/Boundary Layer Interactions," AIAA paper 2002-3232, 22nd AIAA Aerodynamic Measurement Technology and Ground Testing Conference, June 2002.

2. Hou, Y.X., Clemens, N.T. and Dolling, D.S., "Wide-Field PIV Study of Shock-Induced Turbulent Boundary Layer Separation," AIAA paper 2003-0441, 41st Aerospace Sciences Meeting, January 2003.

Summary of Results

Background

Work in a broad range of supersonic separated turbulent flows has suggested that the separation shock foot motion and the expansion/contraction (or pulsation) of the separated flow can be described as a low frequency, large-scale motion superimposed on which is a high frequency, small-scale motion.[1-11] Erengil and Dolling's[9] studies of separation shock foot unsteadiness showed a correlation between the wall pressure fluctuations beneath the incoming boundary layer and the shock foot velocity, from which it was inferred that the small-scale motion of the shock is caused by its response to the convection of turbulent fluctuations through the interaction. Their work also demonstrated that the large-scale motion is a result of the shock's displacement due to the expansion and contraction of the separation bubble. A physical model of the shock unsteadiness can be produced from these observations, where the expansion and contraction of the separation bubble displaces the shock upstream or downstream, while the passage of turbulent fluctuations alters the shock velocity, which integrates to changes in the shock position and accounts for the small-scale high-frequency unsteadiness. While this model offers an explanation for the small-scale motion and a limited explanation for the large-scale motion, it does not address what causes the separation bubble to undergo its low-frequency, large-scale pulsation.

To address this question, McClure[8] and Ünalmis and Dolling[12] made conditional Pitot pressure measurements in the upstream boundary layer and determined that the mean Pitot pressure at a fixed vertical position was lower for upstream shock locations than for downstream shock locations. This observation led to a simple model in which low-frequency variations in the incoming boundary layer *thickness* induce the large-scale shock motion. Chan[13] and Beresh et al.[14] further examined this thickening/thinning mechanism using planar laser imaging techniques. Instantaneous planar laser scattering (PLS) from a condensed alcohol fog was used to obtain images upstream of the interaction in the incoming undisturbed boundary layer simultaneous with pressure signals from transducers used to track the shock foot motion. When analyzed to determine the local mean boundary layer thickness just upstream of the interaction region, the PLS images exhibited no significant correlation between this parameter and the shock location.

Beresh et al.[15] additionally acquired particle image velocimetry (PIV) images simultaneous with pressure data in a Mach 5 compression ramp interaction, similar to the PLS experiment. The resulting vector fields were ensemble averaged based upon the shock foot location as determined from the pressure data, producing conditional mean velocity profiles through the boundary layer. No measurable difference in the boundary layer thickness was found corresponding to different shock foot positions, but the profiles suggested a small difference in the profile shape that may correlate with the shock foot location. Beresh et al.[16] made improved PIV measurements and showed that there was a clear correlation between velocity fluctuations in the lower part of the upstream boundary layer and the shock foot motion. Furthermore, their measurements confirmed the observation that there is no correlation between boundary thickness and shock motion. These results taken as a whole suggest that fluctuations in the upstream boundary layer play an important role in driving the separation shock-foot motion, but the thickening/thinning boundary layer mechanism has little empirical support, at least in Mach 5 compression ramp interactions.

Study Objectives

The discussion above indicates that although a great deal of work has been directed at this issue, the fundamental cause of the low frequency unsteadiness of shock-induced turbulent separation was not known at the time that this research program was initiated. Our work that was supported by a previous ARO grant indicated that in Mach 5 interactions the low frequency unsteadiness was not caused by a thickening/thinning of the upstream boundary layer, and that turbulent fluctuations in the upstream boundary layer are correlated with the motion of the shock foot. The primary objective of this work was to investigate whether the same is true in Mach 2 interactions and to investigate the role of acceleration in the upstream boundary layer on shock-foot motion. To accomplish these tasks a multi-laser, multi-camera PIV system was used to capture wide-field PIV images of the interaction and to conduct two-frame time-sequence PIV to measure flow acceleration. The wide-field PIV was done simultaneously with fast-response pressure measurements to locate the shock-foot position. The simultaneous data give a powerful tool for investigating the flow structure at different phases of the large-scale oscillation cycle.

EXPERIMENTAL APPARATUS AND PROCEDURE

Experimental Facility

All experiments were performed in the Mach 2 blowdown wind tunnel at the University of Texas at Austin. The test section has a constant cross-sectional area of 6×6 in^2. The freestream unit Reynolds numbers was 10^7 ft^{-1}. After transitioning naturally, the incoming boundary layer in the test section was fully turbulent and developed under nearly adiabatic wall temperature flow conditions. The interactions that were studied were generated by a non-full-span 20-degree compression ramp. A schematic diagram of the 28 degree compression ramp mounted on the floor of the test section is shown in Fig. 1.

Fluctuating Pressure Measurements

The pressure measurements were made using five fast response transducers (Kulite model XCQ-062-50A) flush-mounted into a plug that was inserted into the floor of the test section. The transducers had a frequency response of about 50 kHz. The output from each transducer was low-pass filtered at 50 kHz and digitized to 12 bits at 100 kHz by an analog-to-digital converter (LeCroy 6810). The transducers were aligned in the streamwise direction with a center-to-center spacing of 0.115" (2.92 mm). The fluctuating pressure signals were reduced to measurements of the shock foot location using the algorithms detailed by Dolling and Brusniak[3] and Gramann and Dolling.[5]

Multi-Camera, Multi-Laser PIV System

The multi-camera, multi-laser PIV system is shown schematically in Fig. 2. The light source for the system is a pair of dual-cavity, Nd:YAG lasers (Spectra-Physics PIV-400), where each of the cavities (4 in total) can be double-pulsed. Between the two lasers, a pulse train of eight laser pulses can be generated, where the pulse train is repeated at a rate of 10 Hz. The maximum energy per pulse is about 40 mJ for each of the eight pulses. The output beam from the

two separate lasers is combined into a single co-linear beam that is then directed to the test section. The pulse train produced by the lasers depends on whether the system is used for wide-field imaging or time-sequenced imaging. For wide-field imaging, four cameras (Kodak ES1.0), of resolution 1k×1k pixels, are positioned "side-by-side" to image a region of area 21.6×21.6 mm^2, to give a total field of view that was 86 *mm* long by 21.6 *mm* high, with an effective resolution of 4k×1k pixels. To enable the cameras to image overlapping fields-of-view without tilting them, two pairs of cameras were located on opposite sides of the test section, and each pair imaged the flow through a cubic beam splitter. In this case, all cameras imaged the same laser sheet, which was double-pulsed with a time between pulses of 1 μs. For time-sequence imaging, the two cameras were placed on the same side of the test section and imaged the same field-of-view through a cubic beam splitter. Each camera was mounted on an x-y translation stage and a micrometer positioned "tilt" stage that enabled the fields of view to be matched to an accuracy of about a pixel. This level of accuracy was sufficient for the purposes of this study. The two cameras detected particle image pairs separated in time by 40 μs, as compared to the time-between-pulses for each PIV image pair, which was 1 μs.

The scattering for each camera can be differentiated by using a ferroelectric liquid crystal (FLC) shutter (DisplayTech FLC Light Valve) in front of each camera. The FLC shutters are 1" diameter and were custom mounted into C-mount to Nikon lens adapters. The open/close time of the shutters is about 20 ~ 30 μs. Several pulse-delay generators (Stanford Research Systems DG535) were used to synchronize the system and to trigger the different components. For the time-sequence imaging, the laser produced 4 laser pulses per cycle of the laser. The pulses were monitored using a fast photodiode connected to a digital oscilloscope (Tektronix TDS 520C).

TECHNICAL ACCOMPLISHMENTS

Wide-Field PIV

Figure 3a shows a sample composite image of the instantaneous velocity vector field. The composite is formed from four separate PIV images placed side-by-side in software. The individual images that make up a composite image are taken at the same time. A careful viewing of Fig. 3a shows that these wide-field images provide a remarkable amount of information about the global structure of the interaction. In the instantaneous images a relatively abrupt flow deflection, presumably across the separation shock, can be seen in nearly all of the images. To help the reader identify the shock, the locus of points where the vectors first begin to deflect upwards was identified "by eye" and is shown as the solid line in Fig. 3a. The shock is not shown extending to the wall because the flow deflection is not easily discerned within the turbulent boundary layer. From Fig. 3a it is seen that upstream of the shock, the vectors exhibit very little variation in angle or magnitude, as is expected because the RMS velocity fluctuations in the upstream boundary layer are just a few percent of the free stream velocity. Downstream of the shock, the vectors exhibit substantially more variation. What is presumably the separated flow region can also be seen as a region of low velocity. The likely point of separation is shown by an arrow at about x=–30 mm. What appear to be large-scale turbulent structures in the shear layer above the separated flow can also be observed in Fig. 3a.

Interestingly, Fig. 3a shows that although the shock foot is located upstream of transducer 1, the point of separation is not until about 10 mm (or about 0.8δ) downstream of the shock foot. This seems to contradict the view (Gramann and Dolling, 1990) that the instantaneous separation point is at, or close to, the instantaneous shock foot location. Careful inspection of a large number of such vector fields reveals cases where the separation point occurs just downstream of

the shock foot, but in general it is clear that separation is not always induced directly by the shock foot itself. We also observe that the region of "reattachment" exhibits wide variation in its structure. In the majority of images no point of reattachment can be identified at which the flow diverges on each side of it.

The velocity fluctuation field, computed by subtracting the instantaneous image of Fig. 3a from the mean field, is shown in Fig. 3b. In the fluctuation fields, the separation shock can often be easier to identify than in the instantaneous images, because it often appears as a line to which the velocity vectors exhibit a perpendicular orientation. Figure 3b shows that the fluctuations are relatively small in the upstream boundary layer, but are substantially larger in the separated flow and in the recovering boundary layer on the ramp face. In fact, Fig. 3b shows that the fluctuation vectors downstream of the shock foot are nearly all negative, which indicates that we captured a time when a large slug of low momentum fluid was passing through (or induced by) the interaction.

Figure 3c shows a contour plot of u (the x-component of velocity) computed from the vector field of Fig. 3a. In this figure we see the change in the streamwise velocity across the separation shock is about 10 percent. This compares to the approximately 30% change that would be expected for a shock generated by a 20 degree wedge in an inviscid flow. This relatively small change in velocity is expected because the separation shock is initially weak, but gains strength by the coalescence of compression waves, and is not the strength of the inviscid shock until well up the ramp face. We also observe that the shock foot does appear to cause an immediate reduction in velocity, although boundary layer separation clearly does not occur until farther downstream. Figure 3c also shows that the reverse velocities within the separated flow region often exceed 100 m/s, or about $0.2U_\infty$. These large reverse-velocities occur even though the mean velocity shows no indication of reversed flow.

Figure 4a-c shows equivalent sample vector-fields for the case when the shock-foot is at the downstream extent of the intermittent region, i.e. downstream of transducer 5. Figure 4a shows the instantaneous velocity vectors, Fig. 4b the velocity fluctuations and Fig. 4c is a contour plot of the u-velocity. The presumed location of the separation shock outside of the boundary layer is shown as the dark line in Fig. 4a. The shock is seen to be further downstream than in Fig. 4a, which is consistent with what is inferred from the pressure data. One interesting feature of Fig. 4 is that the velocity fluctuations are substantially lower than in Fig. 3 and there is only a very small (or possibly no) region of separated flow. The u-velocity contour plot shows that indeed no reverse-velocities are present for this image. A viewing of many such images indicates that as a general rule, when the shock-foot is downstream, the velocity fluctuations are weaker and the scale of the separated flow is smaller.

To investigate these differences in flow structure with shock-foot position in more detail, ensemble average velocity fields were computed, which were conditioned upon the shock-foot location. These conditional averages are similar to the conditional LDV measurements of Kussoy et al.[17] The conditionally averaged u-velocity contours for far-upstream and far-downstream locations of the shock-foot are shown in Fig. 5. These contours clearly show the flow field is substantially different depending on the location of the shock foot. The region of disturbed flow is clearly larger when the shock foot is upstream. The scale of the 'separated' or at least low-velocity flow is also substantially larger when the shock foot is upstream. This is in general agreement with the conditional LDV measurements of Kussoy et al.[17] who observed a larger separated flow and a farther downstream reattachment distance when the shock was upstream. The ensemble averages of Fig. 5, however, do not show any reversed flow. This is in contrast to the instantaneous vector fields that showed substantial flow reversal. We are not sure at this time if the lack of reverse-flow is related to the fact that our compression ramp is not full span, and

therefore the 3-D relieving effect may weaken the interaction and hence the strength of recirculation.

Figure 6 shows contour plots of conditional-average u_{rms} for shock upstream and downstream conditions. For these plots, the mean used was the conditional mean, i.e. it was computed for a specific shock-foot position. This figure shows that the presence of the separation shock substantially increases the magnitude of the fluctuations over that which appears in the upstream boundary layer. This is a well-known effect that is generally regarded as turbulence amplification due to the shock. Figure 7 also shows that the domain of elevated fluctuations is clearly larger for the shock-upstream case. Furthermore, as was observed from the instantaneous vector fields, the magnitude of the fluctuations is substantially higher (by about 50%) when the shock-foot is upstream as opposed to downstream. In addition, the domain of elevated fluctuations is substantially larger.

The conditional boundary layer velocity profiles based on the shock positions are shown in Fig. 7. Again, the numbers represent the pressure transducers and the letter 'S' indicates the shock foot position. It is clearly shown that the boundary layer shapes change for different shock positions. The profile has a fuller shape when the shock is down stream than it does when the shock is up stream. The boundary layer thickness is 14.3 mm when the shock is up stream, whereas it decreases to 11.8 mm when the shock is down stream. This clearly shows that the boundary layer is thicker when the shock is upstream and thinner when the shock is downstream. This is a very intriguing result, but it is not known why these results differ from what was found by Beresh et al.[16] in Mach 5 compression ramp interactions.

Acceleration Measurement

One objective of the proposed work was to correlate the upstream acceleration, or the rate of change of the velocity profile, to the shock movement. This will be accomplished by using two-frame time-sequenced PIV. In order to make an accurate measure of acceleration, the two pairs of cameras must image exactly the same field of view and take images at different times. Then the difference between the velocity vector fields from different cameras can be obtained to get the acceleration. It is obvious that any spatial mismatch between the cameras will introduce a bias into the measurement.

The timing diagram for the time-sequence PIV is shown in Fig. 8. Two-frame time-sequenced PIV requires that two pairs of laser pulses be generated and each camera must detect only one pair of pulses. Ferroelectric liquid crystal (FLC) shutters are used for this purpose. The minimum open-to-close time of the FLC shutters is about 30-40 microseconds and this sets the minimum time between PIV images as shown in Fig. 8. In order to reduce this bias, the cameras fields of view must be matched to subpixel accuracy. This registration process was done by using Insight 3 from TSI and Matlab's image processing functions. The basic idea was to conduct an *in situ* calibration of the cameras fields of view and use this calibration to correct the PIV images at the post processing stage. The procedure is as follows. The same target grid is imaged by the two cameras. The “dot card” target is composed of equally spaced dots and a single cross in the lower part of the image (an example image is shown in Fig. 9). The cross serves as the origin of the image coordinates. Insight 3 processes the images of the same target from different cameras by generating equations to map the images into a same physical coordinates. These equations are then used to map the PIV particle images to the same physical coordinates. This procedure corrects for variations in translation, rotation and distortion between the two cameras. The corrected images are then processed by normal PIV processing algorithms.

Measurements in a Mach 2 boundary layer have been taken to validate the procedure

described above. Two cameras have been used to image the same field of view. For the first set of experiments the two cameras imaged the scattering induced by the same laser sheets. The resulting flow fields from the two cameras should be identical if there is no mismatch. In the second set of experiments a 40 μs delay was used. The resulting acceleration profiles are shown in Fig. 10. The mean velocity profile change between two cameras with the same timing is shown in Fig. 11a. It is clearly shown that the variation for the mean acceleration is small, as the range is from -0.25 to -0.1 pixels. Ideally, the profile should be exactly zero. If we consider the fact that the accuracy of PIV measurement is on the order of 0.1 pixels, the experimental result shows that the acceleration is indeed zero to within the accuracy of the technique. The mean velocity profile change between two cameras with a 40 μs delay is shown in Fig 11b. Again, the variation is within the range from -0.25 to -0.1 pixels, which is close enough to zero. This is good because ideally, the *mean* acceleration should be zero at each point in the flow. The -0.25 to -0.1 pixels should be considered as the limiting system bias, or uncertainty, in measuring acceleration. The instantaneous velocity profile difference between two cameras with 40 μs delay is shown in Fig. 11c. The instantaneous acceleration is on the order of ±1.5 pixels within the boundary layer. It reduces to the free stream value -0.25 pixels, which is essentially zero. The acceleration within the boundary layer is more than 6 times bigger than the uncertainty. This confirms that the acceleration measurement is good enough for the purpose in this study.

CONCLUSIONS

During the course of this project we have made significant progress toward achieving the goals of the original proposal. The major contribution of this study has been that for the first time, wide-field PIV measurements have been made at different phases of the separated flow pulsation cycle. These measurements have enabled us to make several significant observations. First of all, the global structure of the interaction was found to be substantially different depending on the location of the separation shock foot. When the shock is upstream, the scale of the separated flow, the velocity fluctuations and the domain of perturbed flow, are all substantially larger than when the shock-foot is located downstream. Perhaps the most important finding was that the upstream boundary thickness was clearly seen to be correlated with the shock-foot position. Specifically, the upstream boundary layer is thicker when the shock foot is upstream and thinner when the shock foot is downstream. This result suggests that unsteadiness of the interaction is strongly coupled to variations in the upstream boundary layer.

Furthermore, we have developed the capability to investigate the effect of acceleration in the upstream boundary layer on the shock foot dynamics. It is believed that acceleration may provide an even stronger correlation with shock-foot motion. This effort involved developing a two-image time-sequence PIV technique where the time between images could be varied between 30 and 100 μs. This was a very challenging task because it requires that two separate PIV cameras be registered to sub-pixel accuracy. Nevertheless, the necessary development work has been accomplished and experiments are currently underway to test the acceleration correlation.

Bibliography

1 Gramann, R.A. and Dolling, D.S., "Dynamics of Separation and Reattachment in a Mach 5 Unswept Compression Ramp Flow," AIAA Paper 90-0380, January, 1990.

2 Andreopoulos, J. and Muck, K.C., "Some New Aspects of the Shock-Wave/Boundary-Layer Interaction in Compression Ramp Flows," Journal of Fluid Mechanics, Vol. 180, 1987, pp. 405-428.

3 Dolling, D.S. and Brusniak, L., "Separation Shock Motion in Fin, Cylinder, and Compression Ramp Induced Turbulent Interactions," AIAA Journal, Vol. 27, No. 6, 1989, pp. 734-742.

4 Marshall, T.A., and Dolling, D.S., "Computation of Turbulent, Separated, Unswept Compression Ramp Interactions," AIAA Journal, Vol. 30, No. 8, 1992, pp.2056-2065.

5 Gramann, R.A., and Dolling, D.S., "Detection of Turbulent Boundary-Layer Separation Using Fluctuating Wall Pressure Signals," AIAA Journal, Vol. 28, No. 6, 1990, pp. 1052-1056.

6 Erengil, M.E. and Dolling, D.S., "Correlation of Separation Shock Motion with Pressure Fluctuations in the Incoming Boundary Layer," AIAA Journal, Vol. 29, No. 11, 1991, pp. 1868-1877.

7 Erengil, M.E. and Dolling, D.S., "Unsteady Wave Structure near Separation in a Mach 5 Compression Ramp Interaction," AIAA Journal, Vol. 29, No. 5, 1991, pp. 728-735.

8 McClure, W.B., "An Experimental Study of the Driving Mechanism and Control of the Unsteady Shock Induced Turbulent Separation in a Mach 5 compression Corner Flow," Ph.D. Dissertation, Dept. of Aerospace Engineering and Engineering Mechanics, The University of Texas at Austin, August 1992.

9 Erengil, M.E. and Dolling, D.S., "Physical Causes of Separation Shock Unsteadiness in Shock Wave/Turbulent Boundary Layer Interactions," AIAA Paper 93-3134, July, 1993.

10 Brusniak, L., and Dolling, D.S., "Physics of Unsteady Blunt-Fin-Induced Shock Wave / Turbulent Boundary Layer Interactions," Journal of Fluid Mechanics, Vol. 273, 1994, pp. 375-409.

11 Dolling, D.S., "Fluctuating Loads in Shock Wave/Turbulent Boundary Layer: Tutorial and Update," AIAA Paper 93-0284, January 1993.

12 Ünalmis, O.H. and Dolling, D.S., "Decay of Wall Pressure Field and Structure of a Mach 5 Adiabatic Turbulent Boundary Layer," AIAA Paper 94-2363, June, 1994.

13 Chan, S.C., "Planar Laser Scattering Imaging of Shock Wave Turbulent Boundary Layer Interactions," M.S. Thesis, Dept. of Aerospace Engineering and Engineering Mechanics, The University of Texas at Austin, November 1996.

14 Beresh, S.J., Clemens, N.T., Dolling, D.S., and Comninos, M., "Investigation of the Causes of Large-Scale Unsteadiness of Shock-Induced Separated Flow Using Planar Laser Imaging," AIAA Paper 97-0064, January, 1997.

15 Beresh, S.J., Comninos, M., Clemens, N.T., and Dolling, D.S., "The Effects of the Incoming Turbulent Boundary Layer Structure on a Shock-Induced Separated Flow," AIAA Paper 98-0629, January, 1998.

16 Beresh, S.J., Clemens, N.T. and Dolling, D.S., "The relationship between upstream turbulent boundary layer velocity fluctuations and separation shock unsteadiness," AIAA Journal, Vol. 40, No. 12, pp. 2412-2422, 2002.

17. Kussoy, M.I., Brown, J.D., Brown, J.L., Lockman, W.K. and Horstman, C.C., "Fluctuations and massive separation in three-dimensional shock-wave/boundary layer interactions," Second International Symposium on Transport Phenomena in Turbulent Flows, 1987, The University of Tokyo, Hongo Bunkyo-ku, Tokyo 113, Japan, Oct. 25-29, 1987.

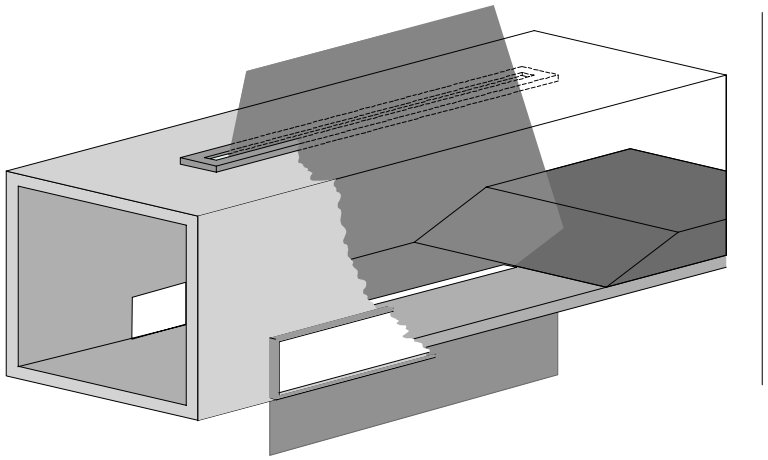

Figure 1. Schematic diagram of the test section with compression ramp.

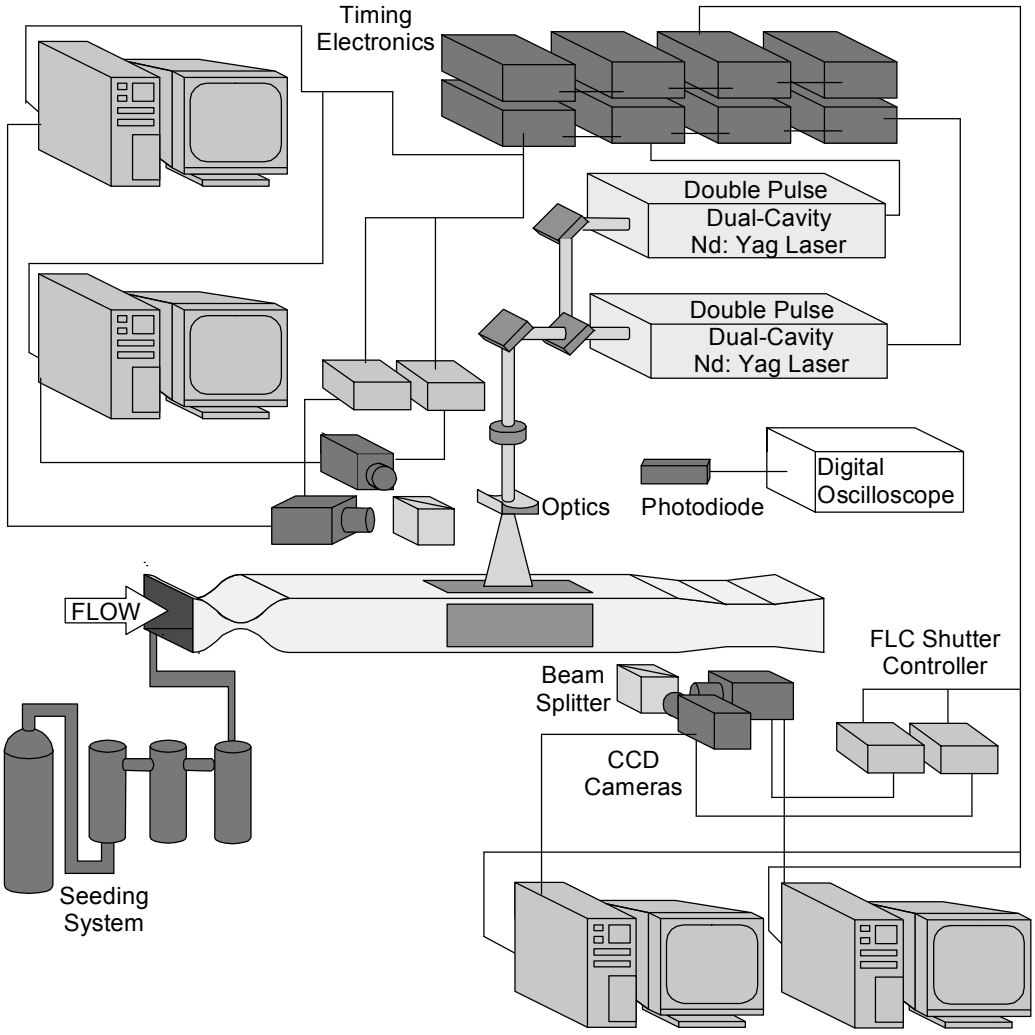

Figure 2. Schematic of multi-laser, multi-camera PIV system setup.

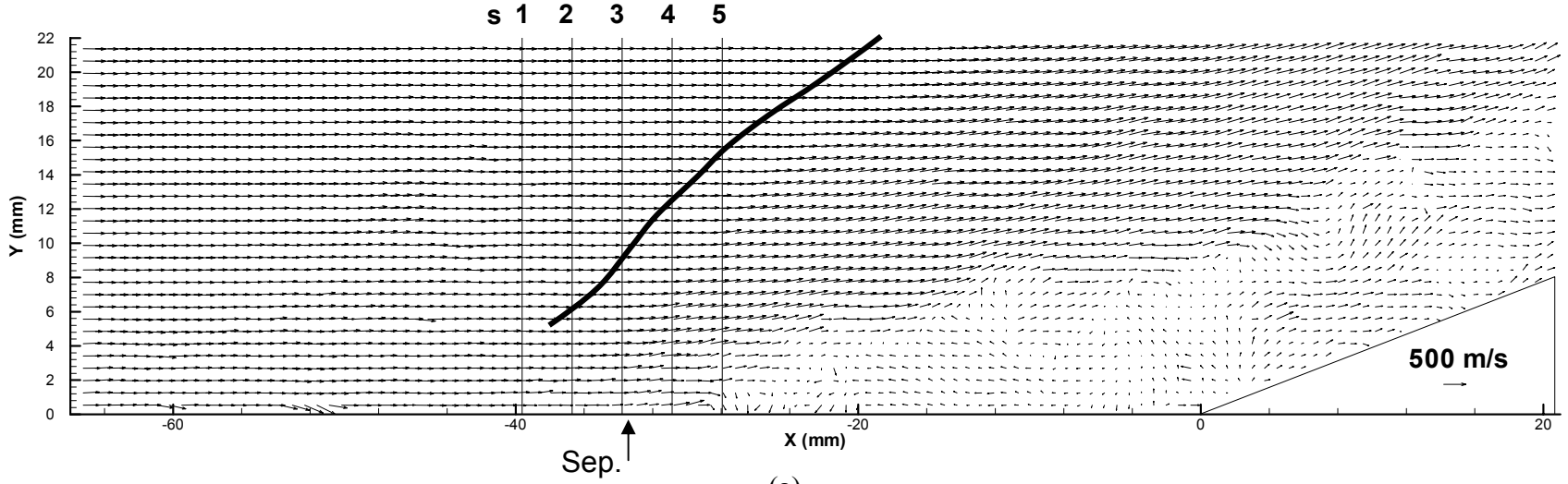

(a)

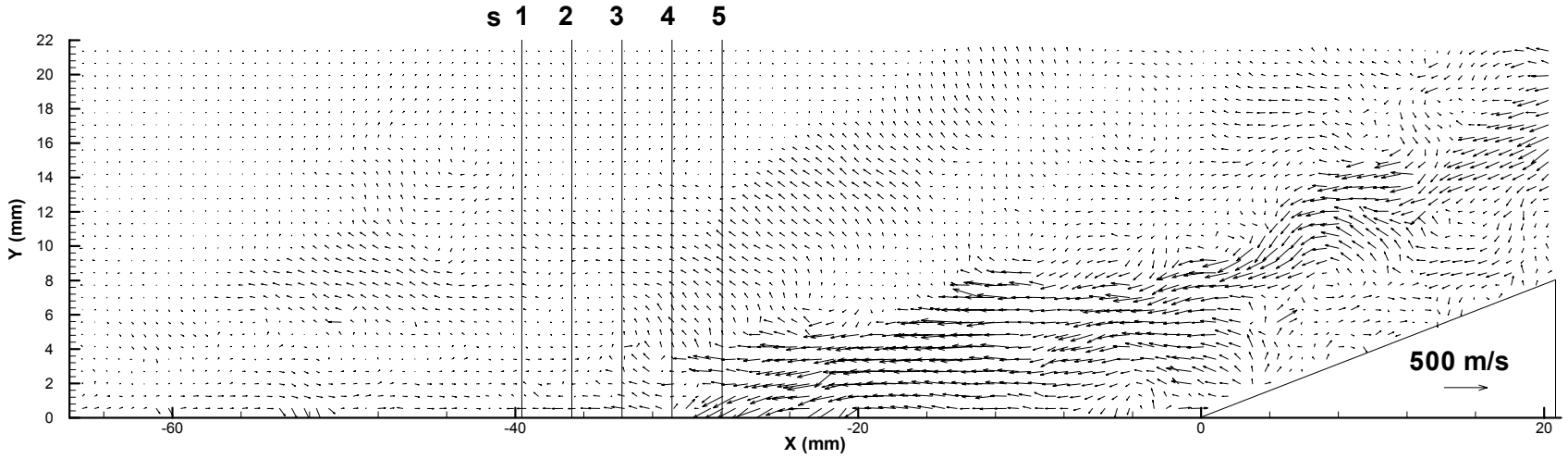

(b)

Figure 3. (See caption next page.)

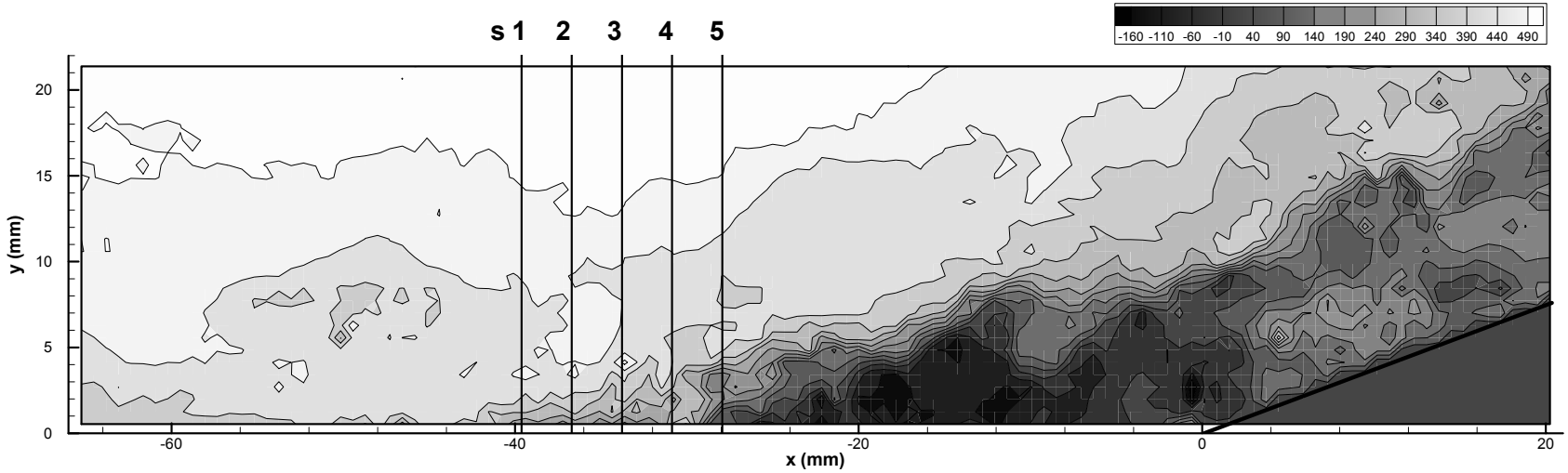

(c)

Figure 3. Sample instantaneous composite velocity fields for the case where the separation shock-foot is upstream of transducer 1. (a) instantaneous vector field, (b) fluctuating velocity vector field, and (c) contour plot of *u*-velocity (units in m/s). (A hand-drawn line is shown on (a) that indicates the upstream location where the velocity vectors outside the boundary layer first begin to deflect upward.)

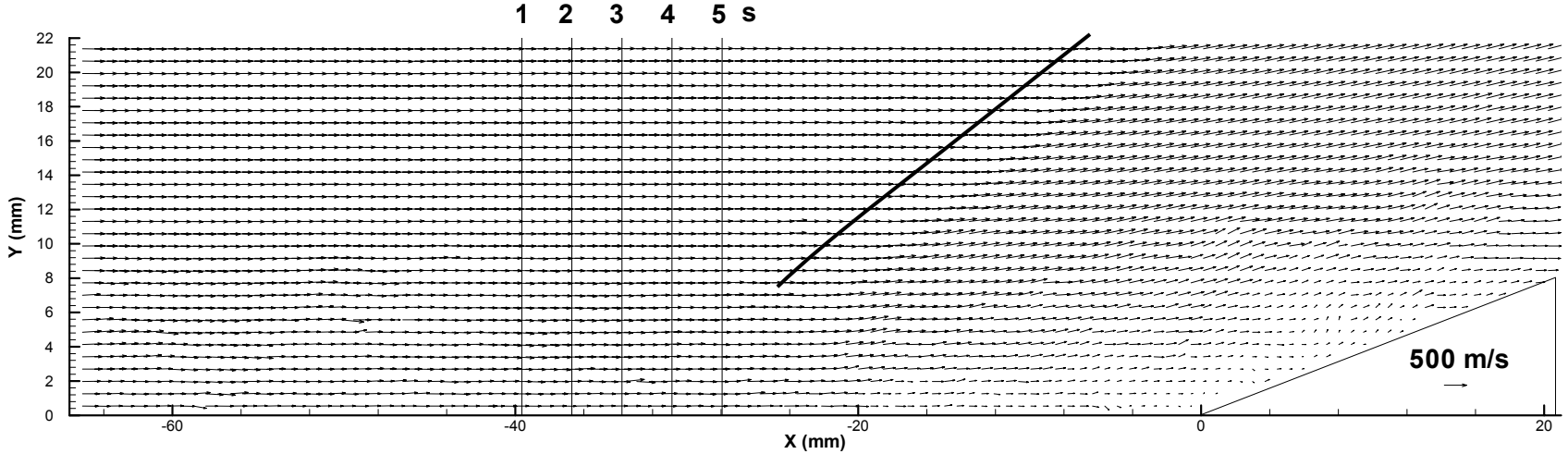

(a)

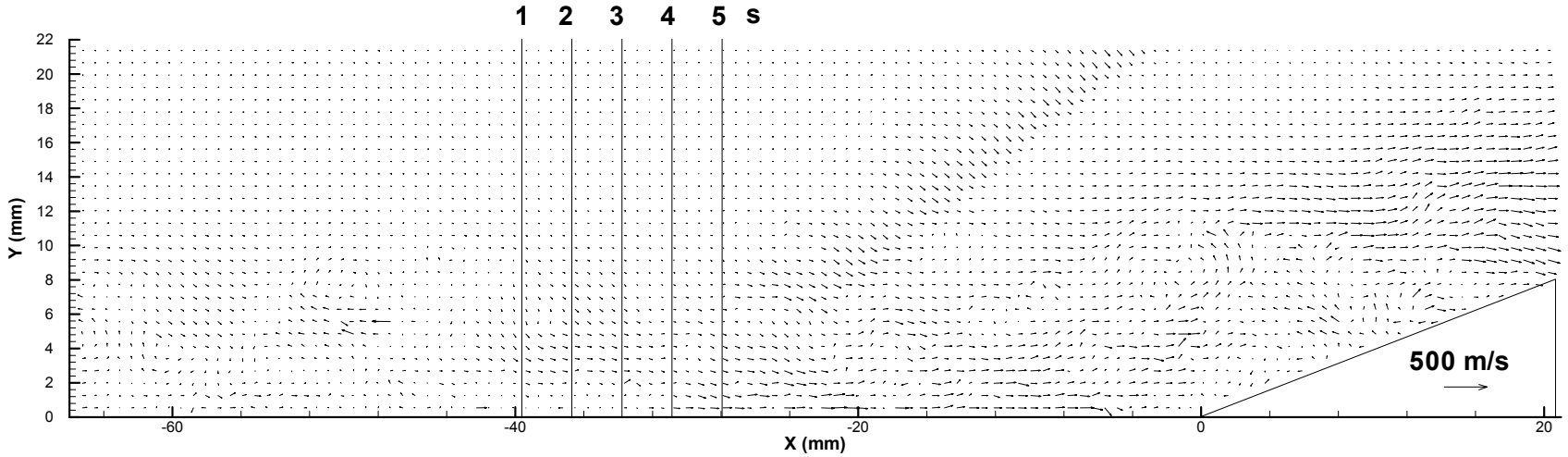

(b)

Figure 4. (See caption next page.)

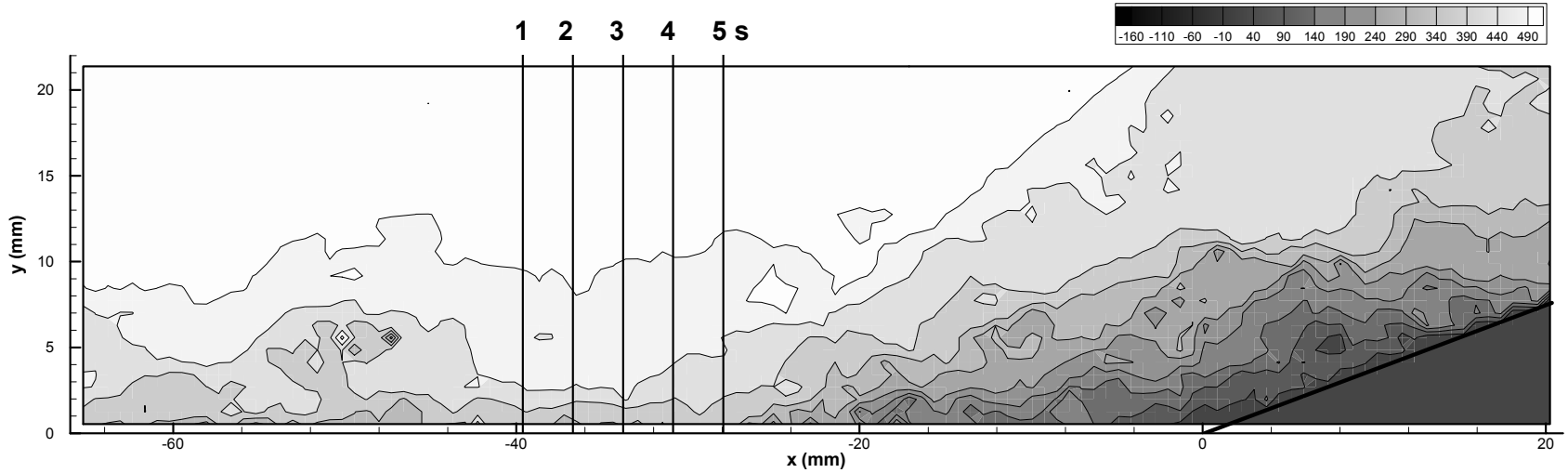

(c)

Figure 4. Sample instantaneous composite velocity fields for the case where the separation shock-foot is downstream of transducer 5. (a) instantaneous vector field, (b) fluctuating velocity vector field, and (c) contour plot of *u*-velocity (units in m/s). (A hand-drawn line is shown on (a) that indicates the upstream location where the velocity vectors outside the boundary layer first begin to deflect upward.)

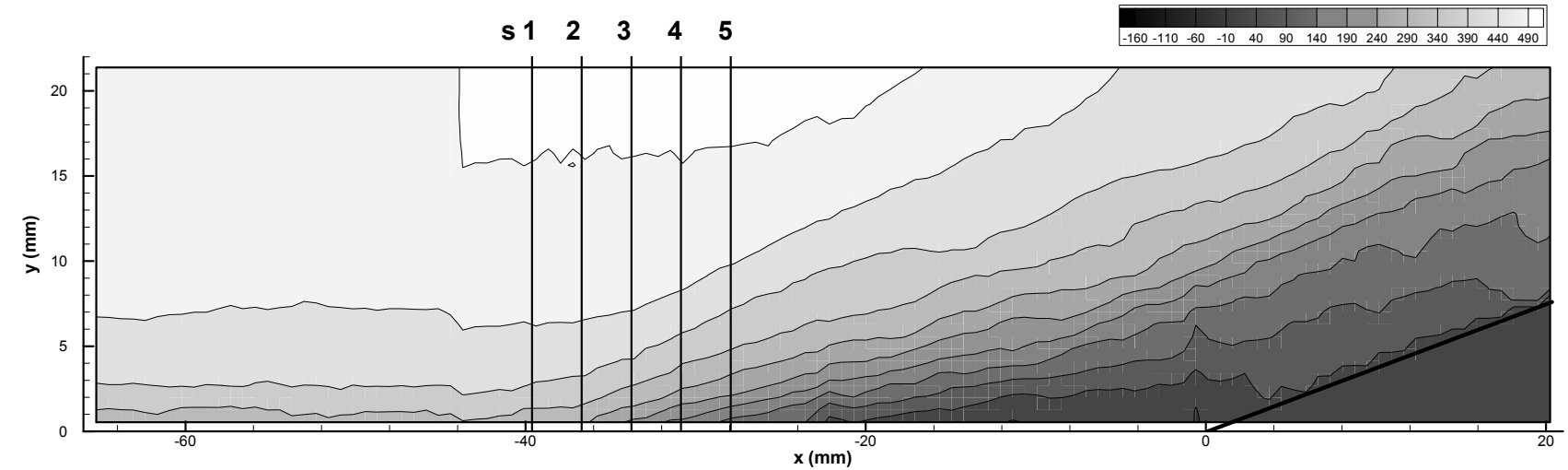

(a)

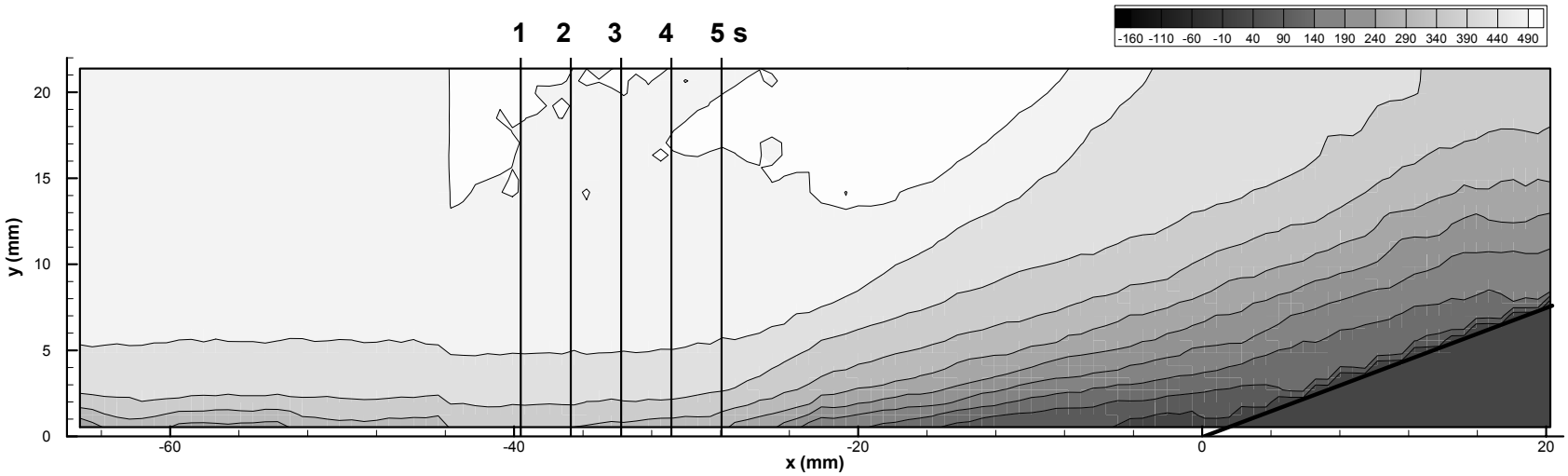

(b)

Figure 5. Conditional-average *u*-velocity contour plots (units in m/s). (a) Shock-foot upstream of transducer 1, (b) Shock-foot downstream of transducer 5.

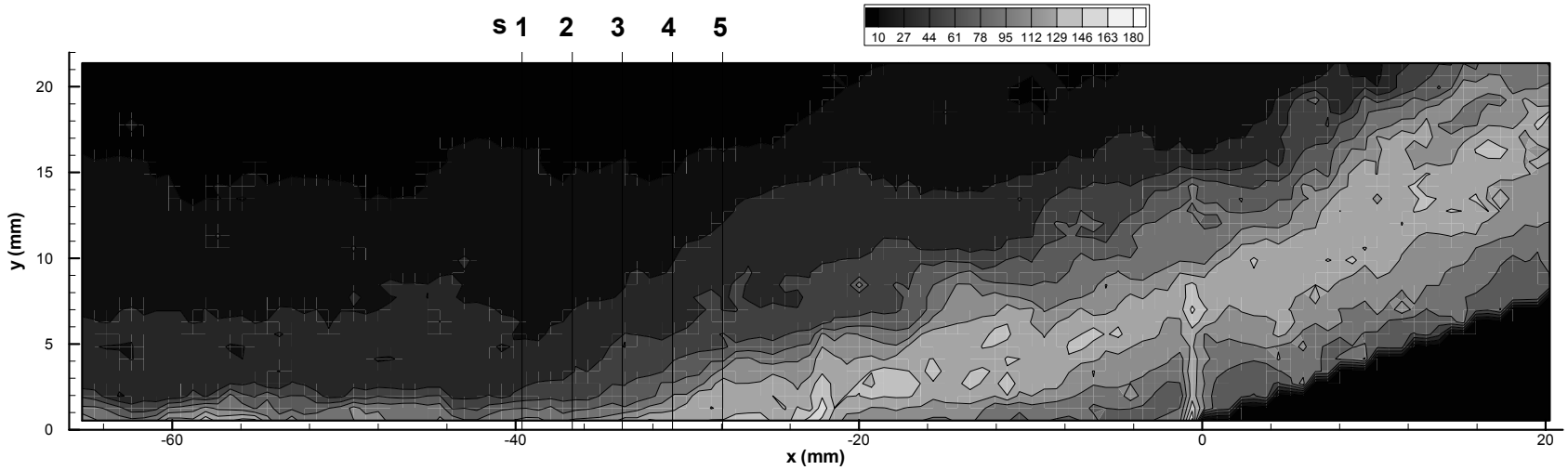

(a)

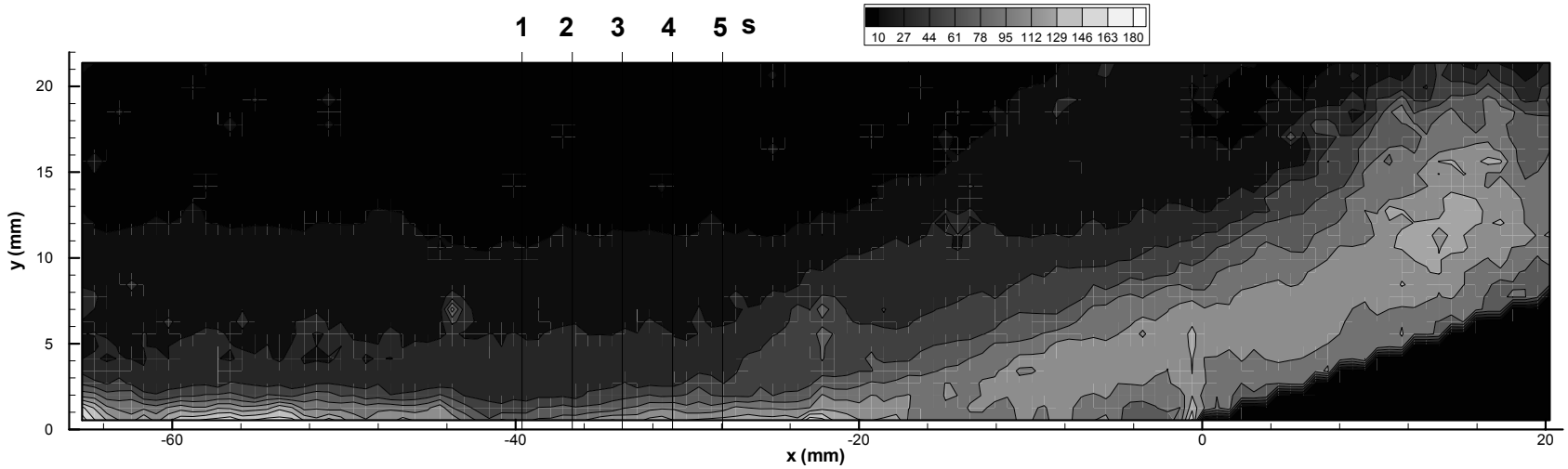

(b)

Figure 6. Conditional u_{rms} contour plots (units in m/s). (a) Shock-foot upstream of transducer 1, (b) Shock-foot downstream of transducer 5.

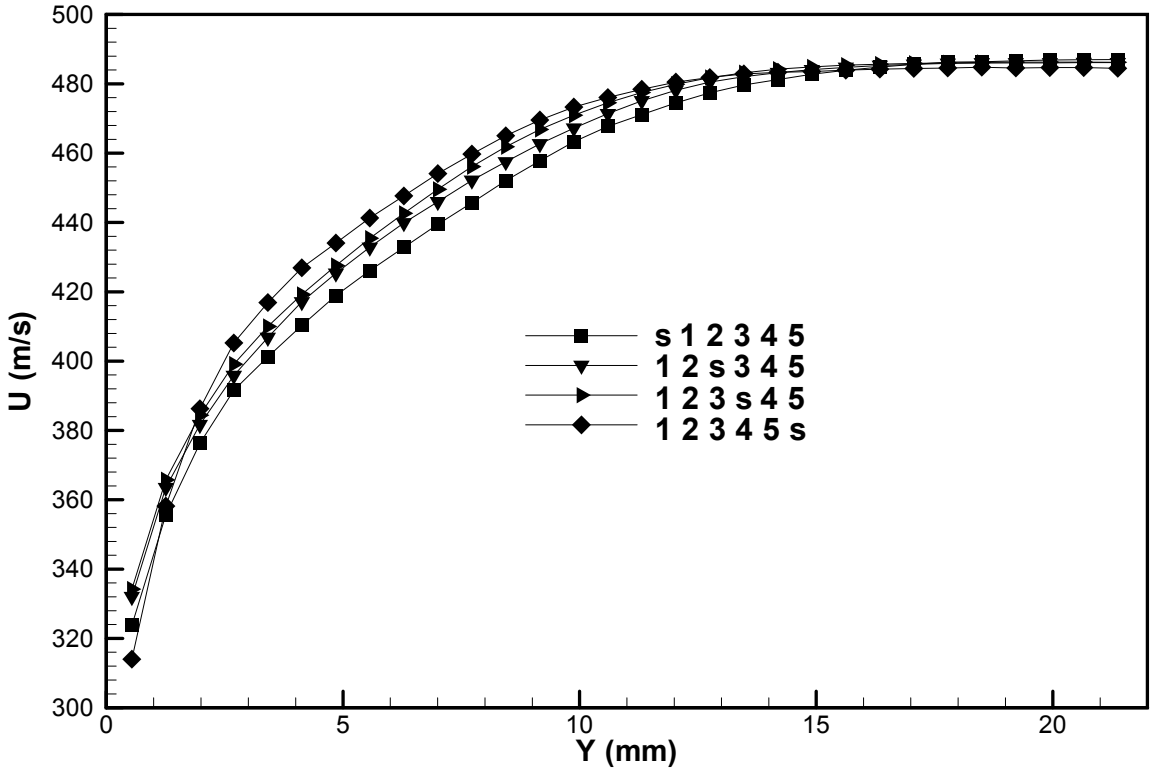

Figure 7. Conditional U velocity profile based on the shock positions.

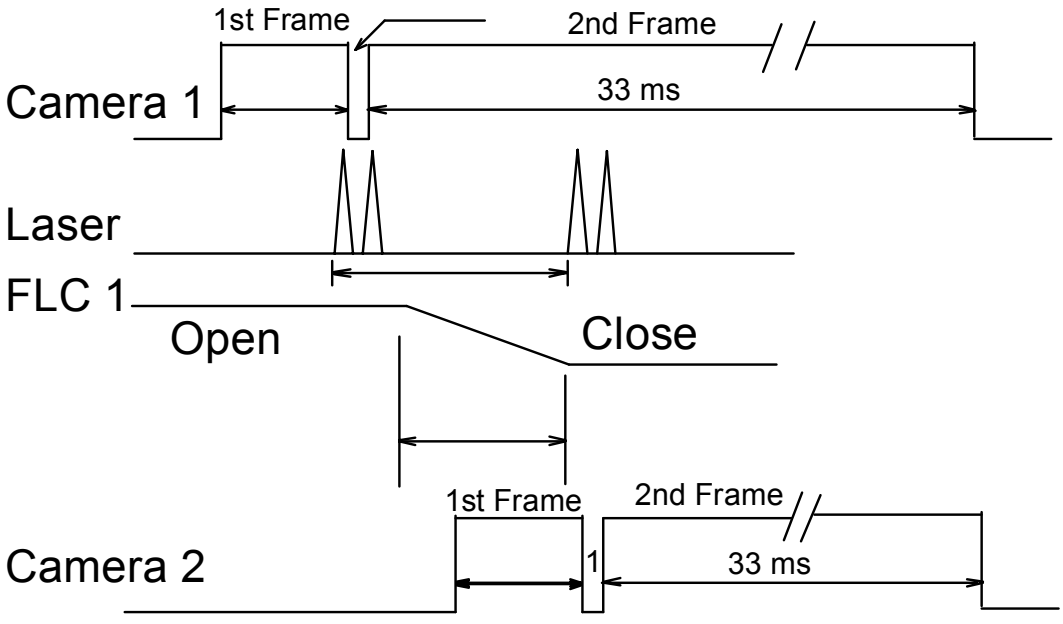

Figure 8. Sample timing diagram for time-sequenced PIV (2 PIV pairs).

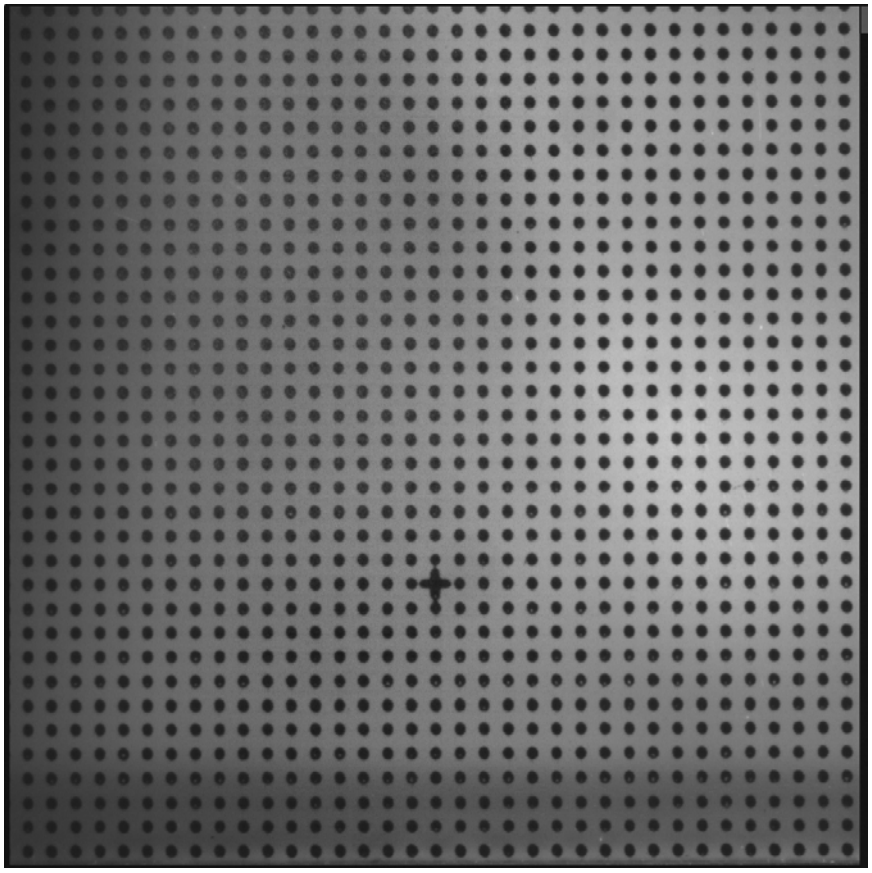

Figure 9. Sample "dot card" target image for acceleration calibration.

(a)

(b)

(c)

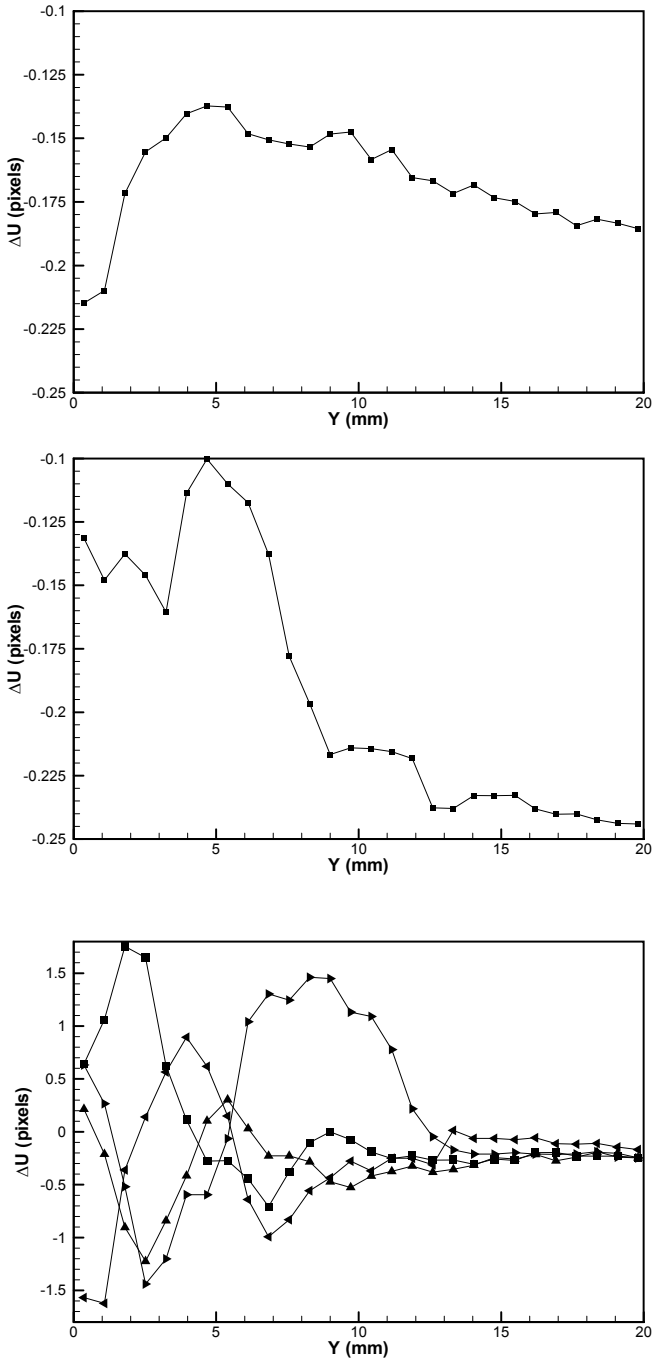

Figure 10. Acceleration profile calibration. (a) Mean velocity profile change between two cameras with the same timing, (b) Mean velocity profile change between two cameras with 40 μS delay, (c) Instantaneous velocity profile change between two cameras with 40 μS delay.